Validation and evaluation of a GATE model for MAMMI PET scanner

Original Article

Azadeh Emami[1,2,3], Pardis Ghafarian [4,5], Hossein Ghadiri[1,2], Parham Geramifar[6], Mohammad Reza Ay[1,2]

[1]Research Center for Molecular and Cellular Imaging, Tehran University of Medical Sciences, Tehran, Iran
[2]Department of Medical Physics and Biomedical Engineering, Tehran University of Medical Sciences, Tehran, Iran
[3]International Campus, Tehran University of Medical Sciences, Tehran, Iran
[4]Chronic Respiratory Diseases Research Center, National Research Institute of Tuberculosis and Lung Diseases, Shahid Beheshti University of Medical Sciences, Tehran, Iran
[5]PET/CT and Cyclotron Center, Masih Daneshvari Hospital, Shahid Beheshti University of Medical Sciences, Tehran, Iran
[6]Research Center for Nuclear Medicine, Tehran University of Medical Sciences, Tehran, Iran

(Received 22 June 2018, Revised 12 October 2018, Accepted 17 October 2018)

ABSTRACT

Introduction: MAMMI is a dedicated PET based on high resolution detectors placed close to the breast. In this study, we presented a GATE model for the simulation of MAMMI scanner and model its performance of the MAMMI based on an adaptation of the NU 4-2008 NEMA standard.

Methods: A detailed of geometry MAMMI system that uses scintillation crystals coupled to position sensitive photomultipliers. The detector ring consists of 12 LYSO detector modules with a scanner aperture of 186 mm. We validated the model against experimental measurement, including spatial resolution, sensitivity, counting rates, noise equivalent count rate (NECR) and scattering pattern.

Results: Overall results showed reasonable agreement between simulation and experimental data. For a breast phantom with a capillary source, the SF reaches 50.9 and NECR is 45 kcps with an activity of 11 MBq, ^{18}F in quad rings. The spatial resolution at the axial FOV of quad rings (2.1 mm axial, 1.8 mm radial, and 1.7 tangential) is slightly better than that measured at the axial center of dual rings (2.1 mm axial, 1.8 mm tangential and radial).

Conclusion: The MAMMI-PET has excellent spatial resolution and high sensitivity for primary breast cancer lesions. The results show performance improvement, especially in the absolute sensitivity, because of the more rings introduced in the MAMMI PET. The performance of the scanner and the validation results are considered to be reasonable enough to support its use in breast cancer imaging.

Key words: Positron emission tomography; Breast; Simulation

Iran J Nucl Med 2020;xx(xx):xx-xx
Published: January, 2020
http://irjnm.tums.ac.ir

Corresponding author: Dr. Mohammad Reza Ay, Department of Medical Physics and Biomedical Engineering, Tehran University of Medical Sciences, Tehran, Iran. E-mail: mohammadreza_ay@tums.ac.ir

INTRODUCTION

Breast cancer is the most common form of cancer diagnosed and the leading cause of cancer death in women. Molecular imaging, particularly positron emission tomography (PET), has become an important diagnostic tool over the last 10 years. Unfortunately, the development of molecular imaging systems for breast cancer has lagged behind that for other oncologic disease [1]. One of the primary reasons being that many whole-body PET scanners do not appear to have adequate resolution for the detection of small lesions in the breast. Whole body PET are not effective for local staging of the breast because their efficiency declines in detecting small lesions [2]. Except for the staging of metastatic disease beyond the breast, PET imaging is not routinely utilized in the evaluation of primary breast cancer.

PET has proven to have better sensitivity and specificity in detecting tumor lesions than x-ray mammography. Dedicated PETs are based on high resolution detectors placed close to the breast where has been the motivation for the development of dedicated systems.

MAMMI is a dedicated high-resolution breast PET developed with convenience of prone positioning during and no need to compress the breast such as conventional mammography MAMMI uses scintillation crystals coupled to position sensitive photomultipliers (PSPMT). The detector ring consists of 12 detector modules (monolithic LYSO crystal) with a scanner aperture of 186 mm and an effective field of view (FOV) diameter of 170 mm and the crystal thickness is of 10 mm. The most important specifications of this system are its transaxial FOV of 170 mm and its spatial resolution of 1.5 mm. The number of ring positions depends on breast size. In patients with large breasts, 3 or 4 ring positions whereas in patients with smaller breasts only two ring positions are acquired. In this work we have evaluated the performance of the quad ring configuration of the MAMMI PET based on the measurements and procedures described for large breasts. The performance of the quad ring configuration has been compared with that of the dual rings configuration [3].

MAMMI is a dedicated high-resolution breast PET, developed in the context of a European project. MAMMI does not require compression of the breast as in conventional mammography. The acquisition is performed in prone position. The obtained 3D images are accurately quantified and characteristic effects of PET images are corrected. The acquisition device contains an arm, from which the ring extends. Precise motion of this arm results in extension of the axial field of view (FOV). The breast of the patient is placed in the ring through an opening in the bed. MAMMI uses scintillation crystals coupled to position sensitive photomultipliers (PSPMT).

The detector ring consists of 12 detector modules in dodecagon configuration with a scanner aperture of 186 mm and an effective field of view (FOV) diameter of 170 mm. Each detector head contains a single monolithic LYSO crystal, a PSPMT, and a proprietary electronic board. The crystal thickness of every device is of 10 mm with a trapezoidal shape. The most important specifications of this system are its transaxial FOV of 170 mm (axial of 35 mm in one shot, up to 170 mm in motion) and its spatial resolution of 1.5 mm. The system allows the user to apply image corrections as they are scattered, random as well as an innovative method for attenuation. The direction of the acquisition is from the chest wall to the nipple. The number of ring positions depends on breast size. In patients with large breasts, 3 or 4 ring positions are used and acquired for 240 seconds each, whereas in patients with smaller breasts only two ring positions with an acquisition time of 300 seconds each are acquired.

In this study we investigate the performance of the PET scanner using the GATE (Geant4 Application for Tomographic Emission) platform. GATE is a Monte Carlo simulation platform based on GEANT 4 libraries that is dedicated to PET and SPECT application [4]. The advantage of this software is that it provides a straightforward scripting interface to model medical imaging system and allows the simulation.

MTHODS

Description of the system

Dual ring MAMMI breast PET: The MAMMI dedicated breast PET has a full ring geometry forming with an aperture of 186 mm. Each detector module consists of a single monolithic LYSO crystal (10 mm thick). The transaxial FOV has a diameter of 170 mm and the axial FOV is 94.4 mm. The detection ring translates axially extending the axial FOV up to 170 mm, in order to image the whole breast.

Quad ring configuration of the MAMMI breast PET: Several modifications have been proposed to upgrade the MAMMI in order to improve its sensitivity and thus reduce the total acquisition time and the dose injected to the patient. In patients with large breasts, 3 or 4 ring positions are used and acquired. In order to extend the axial size of the FOV from 94.4 mm to 170 mm, 4 rings are used. This reduces the number of frames required to image the whole breast, thus reducing the total acquisition. The addition of a second ring also increases the solid angle covered by the detector which leads to increase the sensitivity of the scanner [5].

The Monte Carlo simulation model of MAMMI PET and geometry model

Cylindrical PET GATE model and parameters: The cylindrical PET GATE model has been developed in accordance with the description below (Figure 1).

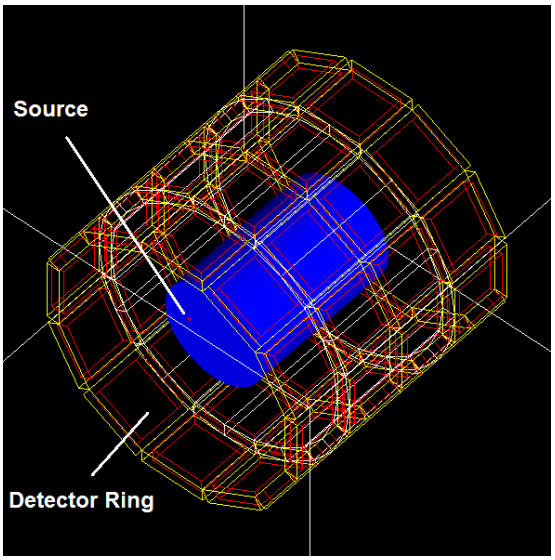

Fig 1. Geometry architecture of 4 Rings MAMMI system- modeled in GATE.

In this work, the main photon physics processes were simulated [6], including photoelectric effect, Compton and Rayleigh scattering. All simulated experiments had a fixed coincidence timing window of 5 ns and energy windows: 250 keV-750 keV. GATE is able to convert photon interactions into counts and reproduce the behavior of the signal processing chain in an analogous manner of a real scanner. The cylindrical MAMMI GATE model has been developed in accordance with the description below (Figure 2). In this work, the main photon physics processes were simulated, including photoelectric effect, Compton and Rayleigh scattering. In this simulation, it is modeled as a Gaussian energy blur with 14% FWHM at 511 keV.

Firstly, we verified the geometry accuracy of the simulation model. Figure 2 showed the transaxial and axial detection position. In figure 2(a), the detection distribution is isotropic and the detector ring is measured 206 mm in diameter (outer diameter), demonstrating that all the detectors have been arranged correctly. In the axial detection (figure 2(b)), there are four spike regions with high counts and three distinct low-count regions between them. The up-and-down count distribution in axial detection is in accordance with detector arrangement, as described in the system configuration. The low-count regions correspond to the gap between each blocks, and the counts come from scatter photons. Besides, the axial detection FOV is around 200 mm measured in Figure 2(b), which accords with system configuration.

Following this, a single is formed and detected on the electronic module. The digitizer chain allows us to simulate the very detailed parameters of the real MAMMI PET setup (Figure 3). After these processing steps, the coincidence events were taken and stored in a ROOT file [7, 8].

Validation study

The phantoms, sources and measurements proposed in NEMA standards to evaluate the performance of the quad ring scanner. The experimental measurements were done following the same procedure as in dual rings of detectors to compare the results [5].

Spatial resolution: The spatial resolution was measured with a 1 mm in diameter ^{22}Na point-like source placed at the center of the axial FOV. Acquisitions were done at radial distances from the center of the scanner up to 70 mm at increments of 5 mm. The full width at half maximum (FWHM) of the reconstructed point source at all three directions has been measured, the effect of the finite size of the source has not been considered in the reported values.

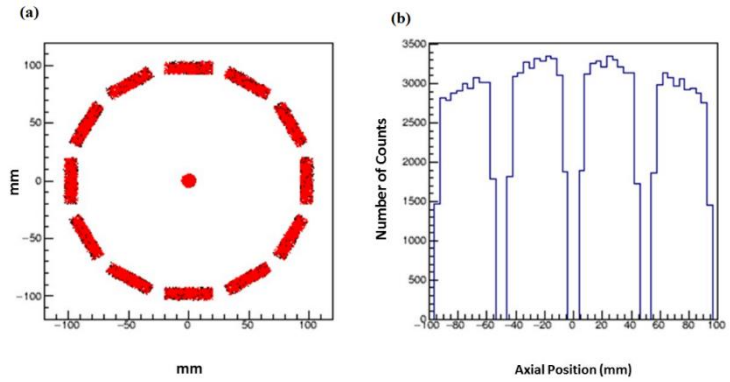

Fig 2. (a) Transaxial and (b) Axial detection position in simulation results.

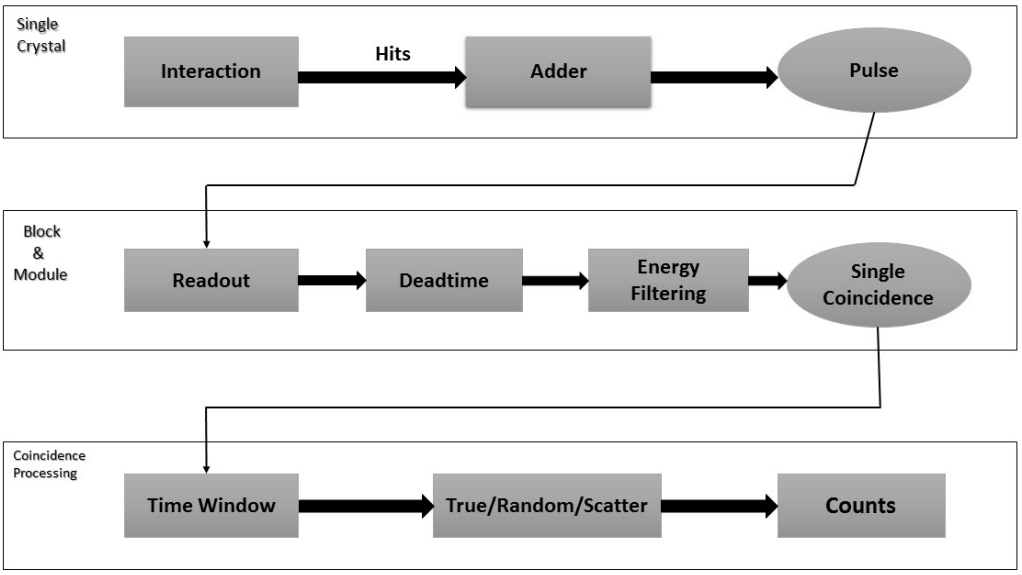

Fig 3. Typical signal processing - simulated in GATE.

Sensitivity: The sensitivity was measured with a 1 mm in diameter ^{22}Na source with an activity of 10 µCi (3.7 MBq), that was moved along the axis of the scanner in step sizes of 5 mm (Figure 4).

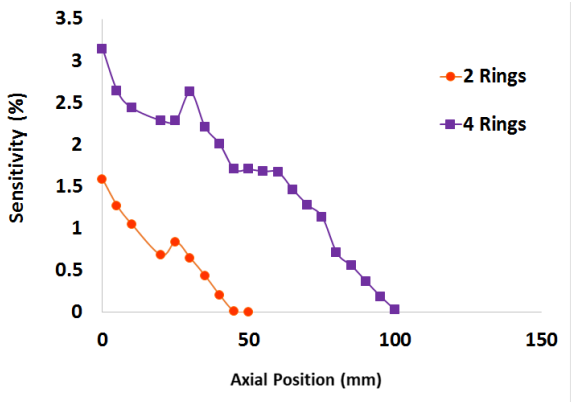

Fig. 4. Comparison of sensitivity measurements with two rings and four rings of detectors.

Counting rate and NECR: NECR and SF of MAMMI scanner were evaluated with a cylindrical phantom containing a line source insert. A phantom composed of breast tissue was simulated and placed at the center of the scanner. A 94.4 (for dual rings) and 170 mm (for quad rings)-long plastic tube with a 3.2-mm diameter placed in a polyethylene scatter phantom. While the phantom was positioned in the FOV center, the F-18-line source was placed 20 mm below the transverse center of the FOV. NECR was calculated for different activity values. NECR and SF were defined by $NECR=T^2/(T+S+KR)$ and $SF=S/(T+S+R)$, where T, S and R are the true, scatter and random coincidence rate, respectively. That k=1 was used to denote a noiseless random correction [9].

Designing with different scintillating material: After the using sensitive photodetectors and of high Z and density scintillating crystals with high light yield, such as LYSO, we have attempted to use other scintillating crystals in PET detectors like BGO, GSO, and LSO. We studied different scintillating crystals materials, BGO, GSO, LSO [10], and LYSO, to determine the most suitable material for a low cost and high performance detector. In this study, we measured and evaluated three different sensitivity data from individual crystal samples [11].

RESULTS AND DISCUSSION

Sensitivity

The addition of the second two rings of detectors leads to an increase of the sensitivity of the scanner (Figure 4). The axial position of the point source is referenced to the center of the FOV in both dual and quad ring configurations of the MAMMI PET. A maximum sensitivity of 3.14% is reached at the center of the scanner with quad ring when considering a (250 keV - 750 keV) energy window and 1.58% if the ring is decreased to two.

The sensitivity achieved at these four local maxima are slightly better than that measured in with two detection rings. This result suggests that the improvement in sensitivity observed in the quad ring configuration is mainly due to the increase of the solid angle covered by the detector.

Spatial resolution

The comparison of the spatial resolution measured with the dual and quad ring configurations of the MAMMI PET are compared, 1.8 mm tangential and radial, and 2.1 mm axial spatial resolution values have been measured in the center of the dual ring MAMMI PET, which are similar to the values 1.7 mm, 1.8 mm and 2.1 mm measured along tangential, radial and axial directions with four ring of detectors. Despite similar values obtained in the center of the scanner, an improvement in spatial resolution is appreciated in the measurements with the quad ring configuration of the MAMMI PET, especially as the point-like source is moved away from the axis of the scanner.

Noise equivalent counts rate (NECR) and count rate

The increase of the axial FOV from 94.4 mm to 170 mm because of the addition of a two second ring of detectors rises the likelihood of detection of scatter events. This enlargement of the FOV leads to an increase of the scatter fraction (SF) from 35.6% to 50.9% when the (250 keV - 750 keV) energy window was chosen (Table 1).

Table 1: Comparison of scatter fraction (%) NECR Peak (kcps @ MBq) measured with the single and dual ring MAMMI PET.

Energy (keV)	**250 - 750**
SF (%)	35.6
Dual Rings NECR (kcps @ MBq)	35 @ 29
SF (%)	50.9
Quad Rings NECR (kcps @ MBq)	45 @ 11

The comparison of NECR peak shows up that the rate of prompts detected in the quad configuration of the MAMMI PET increases that measured for dual ring configuration because of the increase in sensitivity. The higher amount of prompt events detected with the quad ring configuration of the MAMMI PET in comparison with the dual ring configuration is one of the reasons why the NECR peak is reached at 11 MBq which is smaller than that obtained for the dual ring configuration (27 MBq).

Type of detectors and sensitivity

Taking the simulation with dead-time of 500ns, the number of counts was plotted versus axial position in Figure 5 for three different detector materials.

In any imaging situation BGO block detectors have better efficiency than others. Increasing the light collected from BGO crystals to improve energy resolution and sensitivity would greatly enhance their performance.

Scatter component

The Monte Carlo calculation performs a simulated PET acquisition of one bed position (12 detector rings) of the scanner axially centered. Because of the lower number of events in the Monte Carlo generated data sets as compared to the input. The scale factor was derived from the ratio between the scatter plus true simulated data and the uncorrected data from the scanner. The scatter correction is obtained by subtracting the smoothed, scaled calculated scatter estimation from the original data set with normalization (Figure 6).

The quad ring configuration of the MAMMI PET has an axial FOV of 170 mm, which allows to decrease the number of frames required to scan the whole breast. The acquisition time per frame can also be reduced since the sensitivity measured with the quad ring MAMMI PET (3.14%) is twice of that measured with two ring of detectors (1.58%). The improvement in sensitivity is mainly due to the solid angle covered by the quad ring MAMMI PET. The spatial resolution measured at the axial FOV (2.1 mm) in quad ring is the same as in dual ring (2.1 mm) measured.

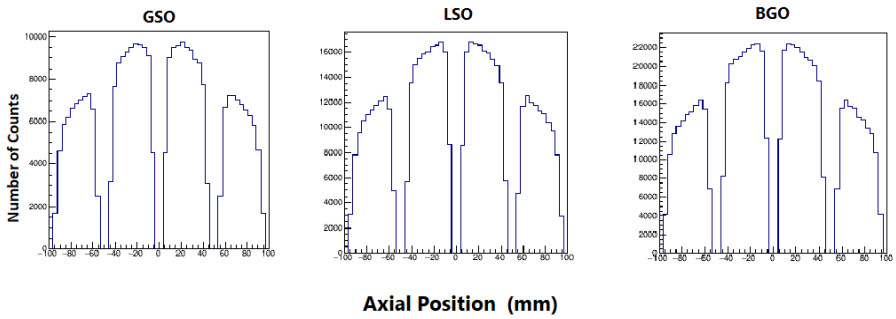

Fig 5. Comparison of the simulated axial sensitivity with data from GSO, LSO and BGO detector materials.

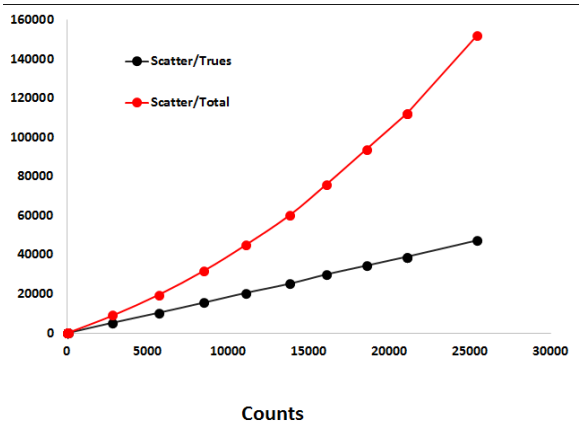

Fig 6. Calculated scatter vs. each event in the simulation (trues = unscattered, total = trues + scattered).

As expected, the increase of the sensitive area leads to a rise of the scatter fraction. The 11 kcps NECR peak achieved with the quad ring configuration increased the (27 kcps) NECR peak measured with dual ring of detectors when the (250 keV -750 keV) energy window is taken into account.

The improvement in sensitivity in the quad ring configuration of the MAMMI PET leads to a substantial increase in the number of counts registered at a given activity, and therefore the NECR peak is reached at an activity of 11 MBq while it was achieved at 27 MBq with the dual ring configuration of the MAMMI PET.

CONCLUSION

The upgrade with a second two ring of detector modules permits to improve the sensitivity of the MAMMI dedicated breast PET. The increase of the detection area and the solid angle covered by the detector is the major cause of the increase in sensitivity observed. The addition of a second two ring of detectors also contributes to enhance the NECR peak values. The rise of the count rate because of the enhancement in sensitivity is one of the reasons for the decrease in the activity at the NECR peak. The good agreement between simulated and measured results demonstrated that the simulation model can efficiently simulate major performance characteristics of MAMMI PET system, and an accurate model of digitizer chain and different designing in material could bring about further improvement. The developed model is accurate enough to be applied in a wide range of applications and it is beneficial for system development. It enables us to evaluate the system performance under various detector materials and can be used to obtain information which is difficult to be measured in practical experiment, such as scatter, and so on [12]. The high spatial resolution and system sensitivity comparable to other designed scanners [13].

REFERENCES

1. Palaniswamy SS, Subramanyam P. Unusual sites of metastatic and benign i 131 uptake in patients with differentiated thyroid carcinoma. Indian J Endocrinol Metab. 2018 Nov-Dec;22(6):740-750.
2. Song HJ, Xue YL, Xu YH, Qiu ZL, Luo QY. Rare metastases of differentiated thyroid carcinoma: pictorial review. Endocr Relat Cancer. 2011 Aug 30;18(5):R165-74.
3. Hassan FU, Mohan HK. Clinical Utility of SPECT/CT Imaging Post-Radioiodine Therapy: Does It Enhance Patient Management in Thyroid Cancer? Eur Thyroid J. 2015 Dec;4(4):239-45.
4. Agrawal K, Bhattacharya A, Mittal BR. Role of single photon emission computed tomography/computed tomography in diagnostic iodine-131 scintigraphy before initial radioiodine ablation in differentiated thyroid cancer. Indian J Nucl Med. 2015 Jul-Sep;30(3):221-6.
5. Campennì A, Giovinazzo S, Tuccari G, Fogliani S, Ruggeri RM, Baldari S. Abnormal radioiodine uptake on post-therapy whole body scan and sodium/iodine symporter expression in a dermoid cyst of the ovary: report of a case and review of the literature. Arch Endocrinol Metab. 2015 Aug;59(4):351-4.
6. Kayano D, Michigishi T, Ichiyanagi K, Inaki A, Kinuya S. I-131 uptake in a thymic cyst. Clin Nucl Med. 2010 Jun;35(6):438-9.
7. Singh AK, Bodolan AA, Gilbert MP. A False Positive I-131 Metastatic Survey Caused by Radioactive Iodine Uptake by a Benign Thymic Cyst. Case Rep Endocrinol. 2017;2017:6469015.
8. Chudgar AV, Shah JC. Pictorial review of false-positive results on radioiodine scintigrams of patients with differentiated thyroid cancer. Radiographics. 2017 Jan-Feb;37(1):298-315.
9. Oh JR, Ahn BC. False-positive uptake on radioiodine whole-body scintigraphy: physiologic and pathologic variants unrelated to thyroid cancer. Am J Nucl Med Mol Imaging. 2012;2(3):362-85.
10. Ranade R, Pawar S, Mahajan A, Basu S. Unusual False Positive Radioiodine Uptake on (131)I Whole Body Scintigraphy in Three Unrelated Organs with Different Pathologies in Patients of Differentiated Thyroid Carcinoma: A Case Series. World J Nucl Med. 2016 May-Aug;15(2):137-41.
11. Garger YB, Winfeld M, Friedman K, Blum M. In thyroidectomized thyroid cancer patients, false-positive I-131 whole body scans are often caused by inflammation. J Investig Med High Impact Case Rep. 2016;4(1):2324709616633715.
12. Hannoush ZC, Palacios JD, Kuker RA, Casula S. False Positive Findings on I-131 WBS and SPECT/CT in Patients with History of Thyroid Cancer: Case Series. Case Rep Endocrinol. 2017;2017:8568347.
13. Deandreis D, Lumbroso J, Al Ghuzlan A, Baudin E, Schlumberger M, Leboulleux S. Abnormal pelvic uptake on post-therapeutic radioiodine (131I) whole-body scan. Eur J Nucl Med Mol Imaging. 2011 Oct;38(10):1957.